Materials Science & Engineering A 789 (2020) 139650

Contents lists available at ScienceDirect

Materials Science & Engineering A

journal homepage: http://www.elsevier.com/locate/msea

Pre-deformation enhanced {10–12} twinning in a zirconium alloy

Xin Chen [a], Qinghui Zeng [b], Weijun He [a,c,*], Qing Liu [a]

[a] College of Materials Science and Engineering, Chongqing University, Chongqing, 400044, China
[b] College of Intelligent Manufacturing Engineering, Chongqing University of Arts and Sciences, Chongqing, 402160, China
[c] International Joint Laboratory for Light Alloys (Ministry of Education), College of Materials Science and Engineering, Chongqing University, Chongqing, 400044, China

ARTICLE INFO

Keywords:
Zr alloy
Twinning
Compression deformation
Texture

ABSTRACT

Twinning is an important plastic deformation mode for zirconium (Zr) and its alloys. In this work, pre-compression followed by orthogonal re-compression, was performed to investigate the effect of pre-deformation on the nucleation of twinning in a textured Zr702 alloy sheet. Microstructures and texture evolution during deformation were examined by electron backscatter diffraction (EBSD) method. It is found that the pre-compression along the normal direction (ND) enhances the activation of {10–12} tensile twins during re-compression along the rolling direction (RD) compared with that in single-step compression along the RD. Moreover, the {10–12} twins preferentially nucleate at grain boundary with relative low misorientation angle (10-30°). When re-compression along the transverse direction (TD) after pre-compression along the ND, the twinning behavior is different from that in re-compression along the RD, which may be attributed to different deformation mechanisms when re-compression along the TD and the RD.

1. Introduction

Zirconium (Zr) and its alloys are widely used in the nuclear power industry due to their low thermal neutron absorption cross section, excellent corrosion resistance, and good comprehensive mechanical properties [1–3]. Zr and its alloys have hexagonal close-packed (HCP) crystal structure at room temperature. Due to the low symmetry of HCP structure, limited independent slip system can be activated in Zr alloys [4,5]. Therefore, twinning is often generated to accommodate the applied strain during plastic deformation [6]. In Zr alloys, the common four types of twins are {10–12}<-1011>, {11–21}<-1-126>, {11–22}<-1-123> and {10–11}<-1011> [7,8]. The former two are tensile twins while the latter two are compressive twins. The twins reorient the crystal lattice by ~85.2° about the {11–20} axis, ~34.8° about the {10-10} axis, ~64.2° about the {10-10} axis, and ~57.1° about the {11–20} axis, respectively [9,10]. Therefore, twinning can significantly change the texture, which has important effect on the irradiation [11], mechanical properties [12,13], corrosion resistance [14,15] of Zr alloys.

Many researches have been performed to investigate the twinning in Zr alloys. O.T. Woo et al. reported that {10–11} twins were activated during the β-quenching process due to martensitic transformation [16]. B.F. Luan et al. found that the {10–12} and {10–11} twins were generated during the slow cooling process from β phase to α phase [8]. G.G. Yapici et al. studied the deformation mechanism of pure zirconium during equal-channel angular extrusion (ECAE) and found that twinning made a significant contribution at room temperature [17]. G.B. Reddy et al. demonstrated that the selection of twinning variants depended not only on the Schmidt factor but also on the geometrical compatibility factors [18]. J.H. Chung et al. reported that pure zirconium can be strengthened by the introduction of high-density twins [19]. O. Muránsky et al. studied the deformation mechanism of Zr–2.5%Nb alloy at room temperature by using in-situ neutron diffraction and found that the {10–12}<10-1-1> tensile twin was activated in the α-phase [20]. M. Knezevic et al. studied the effects of strain rate and temperature on the first twinning and the secondary twinning in high-purity Zr, and found that all of studied twin modes were rate insensitive [21]. W.J. He et al. reported that larger pre-annealing deformation can enhance twin boundary migration at lower annealing temperatures as result of the coherency losses of the twin boundary [10,22]. L. Capolungo et al. reported a strong correlation between twin variant selection and crystallographic orientation [5].

The activation of twin is affected by many factors, for instance, the grain orientation [23,24], grain size [25], deformation temperature [26,27] and strain rate [28,29]. Twinning in Zr alloys may be also affected by the pre-deformation. H.L. Yang et al. reported that the {10–12} twins

* Corresponding author. College of Materials Science and Engineering, Chongqing University, Chongqing, 400044, China.
E-mail address: weijun.he@cqu.edu.cn (W. He).

https://doi.org/10.1016/j.msea.2020.139650
Received 26 February 2020; Received in revised form 9 May 2020; Accepted 24 May 2020
Available online 1 June 2020

activated in uniaxial tension were composed of slip-independent twins and slip-assisted twins [30]. The slip-independent twins were activated when the global stress surpassed the required critical stress, while the slip-assisted {10–12} twins were generated thanks to the local stress concentration near the grain boundary [30]. During pre-deformation, many slips were activated and complex intergranular stress was accumulated, which may significantly affect the activation of the twinning during subsequent deformation. During the forming processes of Zr alloys, for example pilger rolling, materials successively experience different strain and stress states. Therefore, it is important to investigate the effect of pre-deformation on the activation of twinning during subsequent deformation, which is, however, not emphasized in previous work.

In this work, two steps of compressions were performed on a Zr alloy sheet. The pre-compression was conducted along the normal direction (ND), while the re-compression was conducted along the rolling direction (RD) or the transverse direction (TD). The selection principle of the loading direction was that the twin would not be activated in the pre-deformation, while the re-compression was easy to activate twin. Microstructures and texture before and after deformation were carefully characterized by electron backscatter diffraction (EBSD). The motivation of this study is to investigated the effect of pre-compression on the activation of twinning during subsequent compression, which is important to reveal the twinning in deformation undergoing strain path change.

2. Experiment and methods

Commercial pure zirconium (Zr702) rolled plate, with the thickness of 4.4 mm, was used as the experimental material in this work. The initial microstructure is composed of fully recrystallized grains, as shown in Fig. 1. The initial average grain size is approximately 25 μm, which was measured by linear intercept method based on electron backscatter diffraction (EBSD) data. Grains are equiaxed and no twin can be observed, as indicated in Fig. 1(a) and (c). In Fig. 1(c), the {10–12} tensile twin boundary is superimposed on the band contrast map (indicating the image quality with gray scale) and is marked with red solid line (if there is any twin). This band contrast map superimposed with twin boundary is denoted as twin boundary map because it is mainly dedicated to display the amount of twin boundary in the current work. The distribution of the misorientation angle of boundary is presented in Fig. 1(b). The maximum peak appears around the 30-40°, which is often reported in recrystallized Zr alloy [31]. The texture of the as-received plate is a typical split basal texture, as shown in Fig. 1(d).

To carry out compressive deformation, small sample with size of 5 mm (rolling direction, RD) × 4 mm (transverse direction, TD) was cut from the as-received Zr702 plate. Two-step compressions were conducted. The first step of compression (pre-compression) was conducted along the ND of the Zr702 plate, while the second step of compression (re-compression) was conducted along the RD or the TD. For the pre-compression, three strain levels (5%, 10% and 20%) were applied. While, during the re-compression, 10% was applied regardless of the compression direction. All compressions were performed at room temperature by using Shimadzu AG-X50kN mechanical performance test machine, and the compression rate was 10^{-2} mm/s. For comparison, single-step compressions along the RD and the TD, with reduction ratio 10%, were also carried out. For the sake of convenience, samples are named after the compressive strain and the loading direction. For example, CN-10%-CR-10% sample means that the sample is pre-compressed 10% along the ND and then re-compressed 10% along the

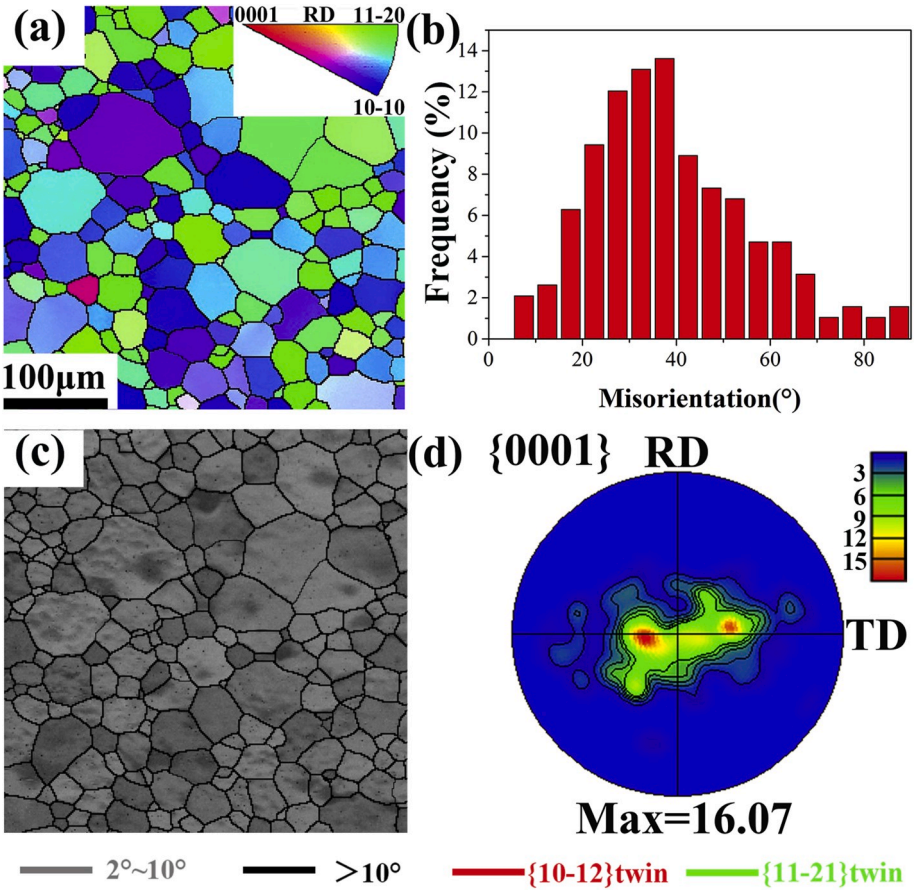

Fig. 1. Initial microstructure of the experimental material: (a) orientation imaging map (b) misorientation angle distribution, (c) band contrast map superimposed with twin boundary (twin boundary map) and (d) {0001} pole figure.

RD.

To characterize the microstructure by EBSD, the surface of the sample was electrolytic polished to obtain a fresh surface. The prepared samples were observed by TescanMir3 Field emission scanning electron microscope equipped with an Oxford Instruments-HKL Technology Nordlys EBSD system. Experimental voltage was 20 KV, and working distance was 12 mm. The observed area was about 400 μm × 400 μm, which was located at the center of the RD-ND plane. The indexing step size was 1.5 μm. The obtained data was analyzed by commercial available package channel 5.

3. Results

3.1. Microstructures after pre-compression along the ND

The orientation imaging maps and twin boundary maps (band contrast map superimposed with twin boundary distribution if there is any twin) of Zr702 after 5%, 10% and 20% pre-compression along the ND are shown in Fig. 2. In the orientation imaging map and twin boundary map, ordinary high angle grain boundary (misorientation angle >10°) and low angle grain boundary (2° <misorientation angle <10°) are represented by dark coarse line and gray fine line, respectively. Fig. 2 indicates that no twin is activated after the pre-compression. It was reported that the main deformation mechanisms were prismatic <a> and pyramidal <c+a> slipping when compression along the ND of Zr sheet with strong split basal texture based on slip trace analysis as well as VPSC simulations [32,33]. With the increase of strain (5%–20%), color gradients are observed in most of grains, which demonstrates that the local orientation within a grain is no longer uniform. The misorientation inside a grain is generally associated with non-uniform deformation among different grains [4]. The non-uniform deformation may induce complex stress/strain state in local region other than the nominal applied uniaxial compressive state. The distributions of the misorientation angle of the CN-5%, CN-10% and CN-20% sample are shown in Fig. 2(g)–(i). The fraction of the low angle boundary (LAB, <10°) increases with the increase of the applied strain, which is consistent with the more and more sub-boundaries observed in Fig. 2 (a)–(c).

3.2. Microstructures after compression along the ND and RD

For comparison, the orientation imaging map and twin boundary map of single-step compressed sample along the RD are firstly show in Fig. 3(a) and (e). It shows that {10–12} twins are activated after single-step compression along the RD. Since the *c-axis* is roughly parallel to ND in the initial plate (basal texture as indicated in Fig. 1(d)), the *c-axis* is mainly subjected to extension strain when compression along the RD, which is easy to active the {10–12} tensile twin. Actually, the activation of {10–12} tensile twin in compression along the RD was also reported in our previous studies [10,33].

The orientation imaging maps and twin boundary maps of re-compressed samples along the RD (after pre-compression along the ND) are displayed in Fig. 3(b)–(d) and Fig. 3(f)- (h). It indicates that many twins are also activated in the re-compressed samples regardless of the applied strain in the pre-compression stage. Actually, compared with the single-step compressed sample (RD-10%), more twins are activated

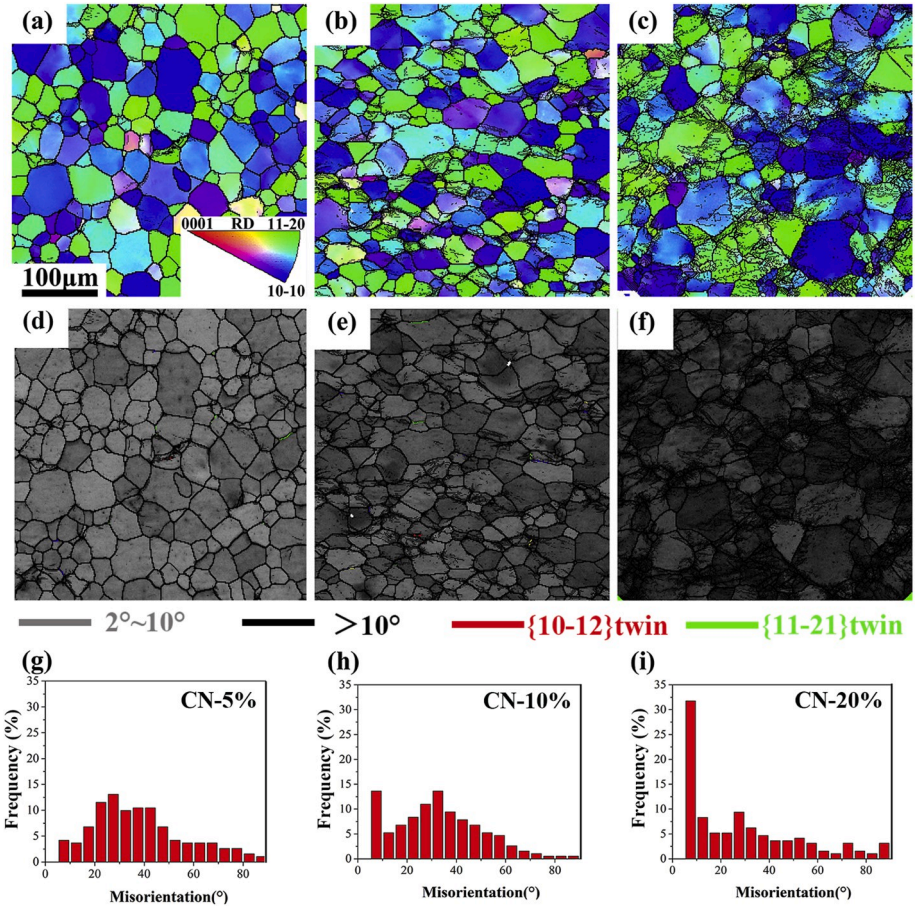

Fig. 2. Microstructures of pre-compressed samples: orientation imaging map of (a) CN-5%, (b) CN-10% and (c) CN-20%, and twin boundary map (band contrast map superimposed with twin boundary distribution if there is any twin) of (d) CN-5%, (e) CN-10% and (f) CN-20%, and misorientation angle distribution for (g) CN-5%, (h) CN-10% and (i) CN-20%.

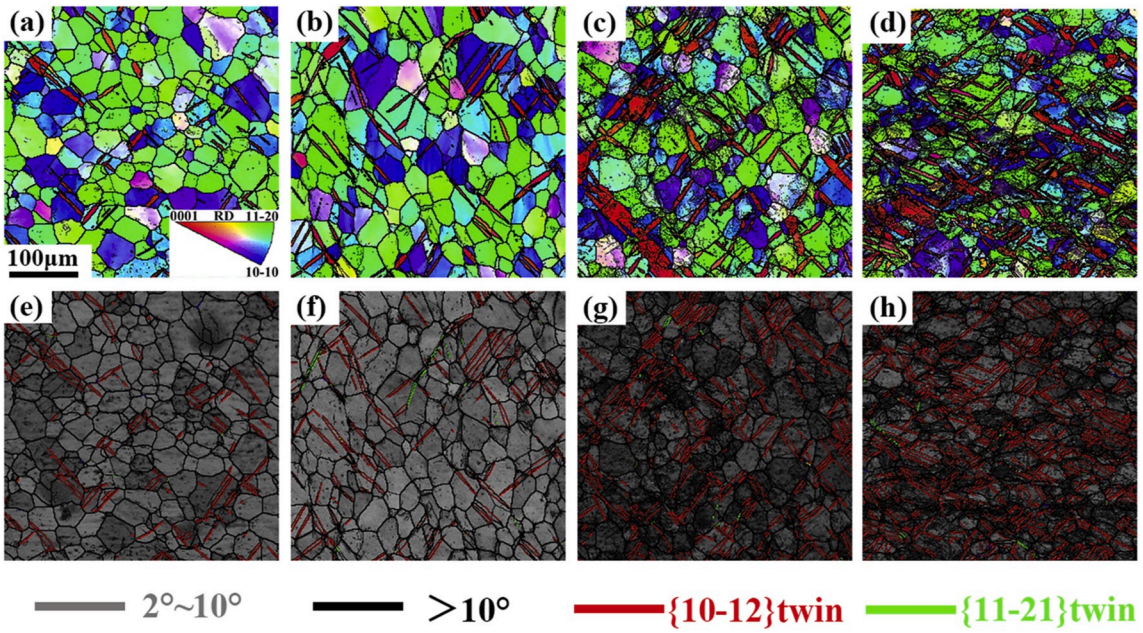

Fig. 3. Microstructures of compressed samples along the RD: orientation imaging map of (a) CR-10%, (b) CN-5%-CR-10% (c) CN-10%-CR-10% and (d) CN-20%-CR-10%, twin boundary map of (e) CR-10%, (f) CN-5%-CR-10% (g) CN-10%-CR-10% and (h) CN-20%-CR-10%.

in the re-compressed sample along the RD, as demonstrated by the quantitative statistical results in Fig. 4. The twin number density in CR-10% and CN-5%-CR-10% sample is 36.5% and 50.5%, respectively. That means the pre-compression along the ND can enhance the activation of {10–12} tensile twin during re-compression along the RD. In addition, the higher the amount of the pre-deformation strain, the more obvious the promotion effect is. For example, the twin number density in CN-20%-CR-10% is 82.2%, which is more than two times higher than that in CR-10%. It is worth to note that the twin number density is defined as the ratio between the number of grains with twin activation to the observed total number of grains. Actually, if count the twin area fraction, it shows same evolution tendency as the twin number density.

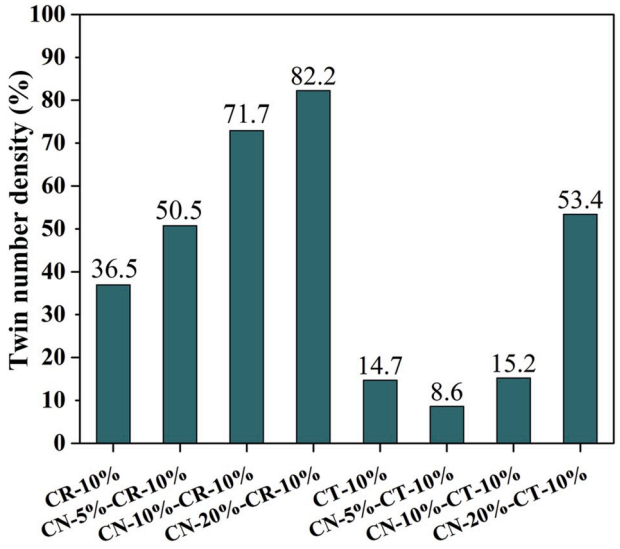

Fig. 4. Quantitative statistics of the {10–12} twin number density in compressed samples along the RD and TD. The twin number density is defined as the ratio between the number of grains with twin activation to the observed total number of grains.

3.3. Microstructures after compression along the ND and TD

As reference information, Fig. 5(a) and (e) show the microstructure of CT-10% sample, which was prepared by single-step compression along the TD. It indicates that {10–12} twins are also activated after compression along the TD. However, the twin number density (14.7%) for CT-10% is less than that in CR-10% (36.5%), as shown in Fig. 4. This may be attributed to the initial split basal texture (Fig. 1(d)). The *c-axis* of grains are roughly parallel to ND but tilting about 10–20° to TD. So, when compression along the TD, the Schmid factor for the tensile twinning will be lower than that along the RD, thus leading to less {10–12} twin activation.

Fig. 5(b)–(d) and Fig. 5(f)-(h) present the microstructures of re-compressed samples along the TD. It indicates that tensile twinning is also activated during re-compression along the TD after pre-compression along the ND. However, it is worth to note that the pre-deformation along the ND is not always enhance the tensile twin activation when re-compressing along the TD. Fig. 4 indicates that the twin number density in CN-5%-CT-10% (8.6%) sample is less than that in CT-10% (14.7%). So, small (5%) pre-strain along the ND actually hinders the twin activation during the re-compression along the TD, which is different from the tendency during re-compression along the RD. The twin number density in the TD re-compressed sample increases with the increase of the pre-compression along the ND. When the pre-strain is 20%, as shown in Fig. 4, the twin number density (53.4%) is even higher than that in CT-10% (14.7%). Therefore, large pre-deformation (20%) along the ND can also enhance the activation of tensile twinning during the re-compression along the TD.

3.4. Texture evolution

{0001} pole figures are presented in Fig. 6 to show the texture evolution after different compression deformations. It indicates that the pre-compression along the ND has small effect on the orientation of the basal pole. So, the significant effect of the pre-deformation along the ND on the subsequent tensile twinning activation during re-compression along the RD or TD may be not related with the texture change. We will continue to evaluate the potential effect of the texture change on the subsequent twinning by calculating the Schmid factor in section 4.1.

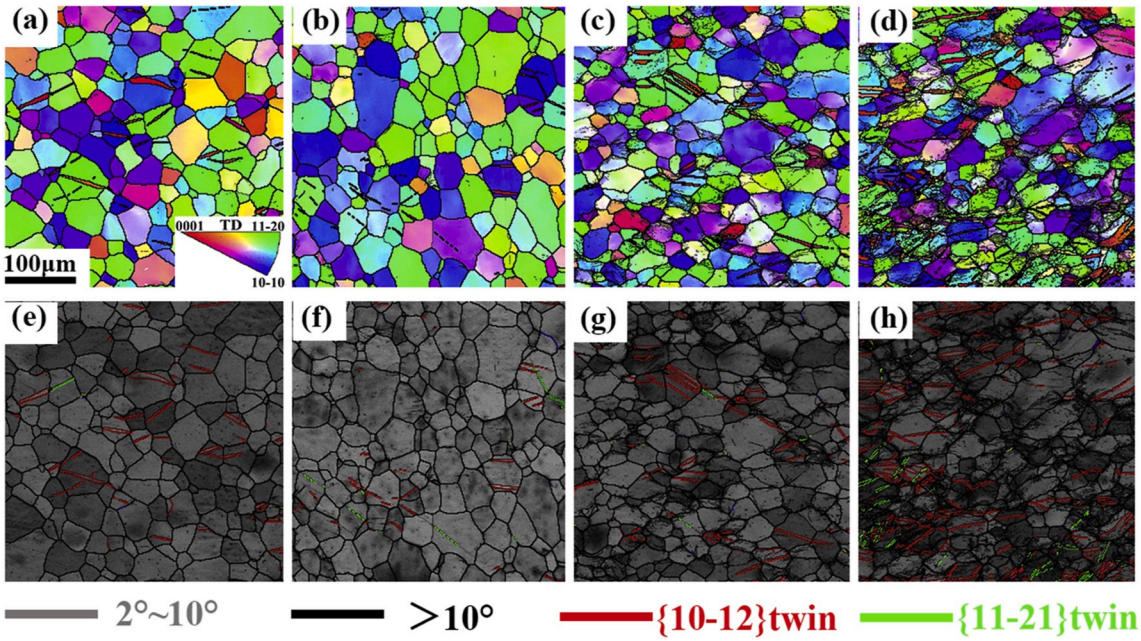

Fig. 5. Microstructures of compressed samples along the TD: orientation imaging map of (a) CT-10%, (b) CN-5%-CT-10% (c) CN-10%-CT-10% and (d) CN-20%-CT-10%, and twin boundary map of (e) CT-10%, (f) CN-5%-CT-10% (g) CN-10%-CT-10% and (h) CN-20%-CT-10%.

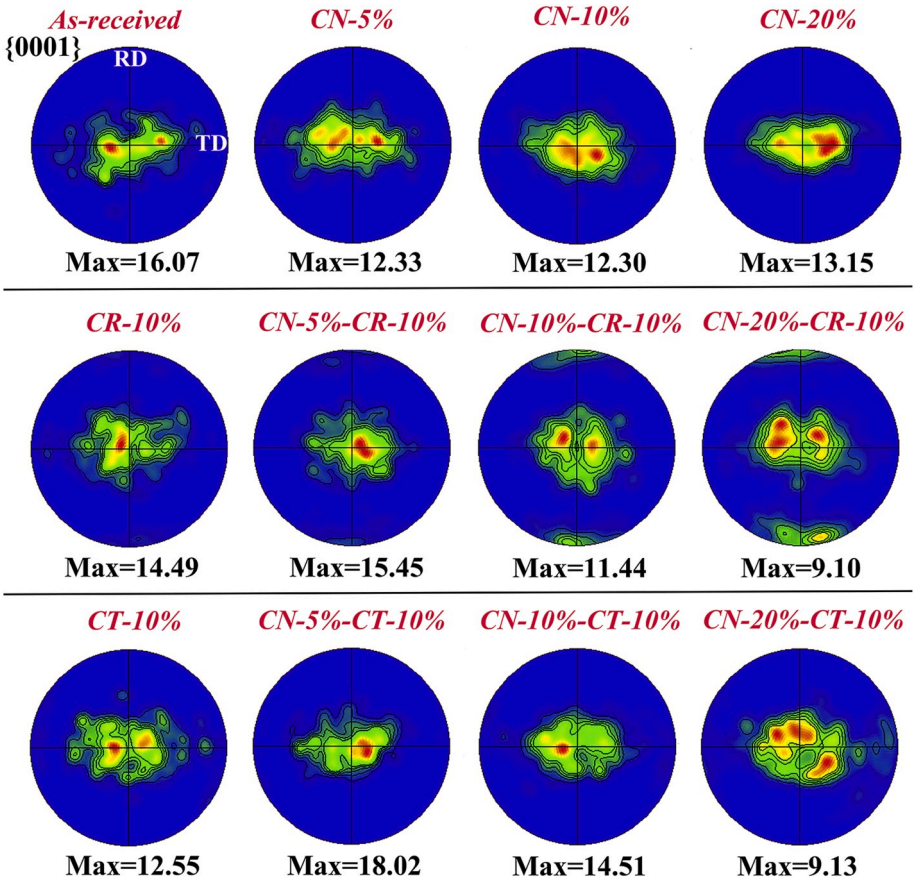

Fig. 6. {0001} pole figures after compression along different directions.

After the RD compression, a new texture component {0001}//RD is formed due to the activation of tensile twins [10,33]. In fact, texture component {0001}//TD should also be formed as result of the activation of tensile twinning after compression along the TD. However, the texture component {0001}//TD is not obvious in the {0001} pole figure, which is caused by the low twin area fraction. With the generation of texture component {0001}//RD or {0001}//TD, the texture component {0001}//ND is weakened.

4. Discussions

Experimental results indicate that the pre-deformation along the ND has significant effect on the activation of tensile twin during subsequent compression along the RD and TD. In addition, the specific influence changes with the change of the subsequent compression direction and the amount of the pre-deformation. In this section, four factors, including the grain orientation, misorientation angle of grain boundary, local stress and anisotropy, are analyzed to reveal the influencing mechanism of the pre-deformation on the subsequent twinning.

4.1. Effect of orientation change induced by the pre-deformation on the twinning during re-compression

Fig. 4 indicates that the pre-deformation along the ND has significant effect on the subsequent twinning. One of the possible mechanisms is that the texture may be changed by the pre-deformation along the ND. However, Fig. 6 shows that no obvious texture change can be noted after the pre-deformation along the ND. To quantitatively show the possible effect of the tiny texture change induced by the pre-deformation on the twin activation during re-compression along the RD or TD, the Schmid factor is calculated. Fig. 7 shows the Schmid factor distribution maps of {10–12} tensile twin if compressing along the RD and TD for the as-received sample and the pre-compressed samples. Schmid factors are computed based on the orientation maps shown in Fig. 1(a) (as-received sample) and Fig. 2(a)–(c) (pre-compressed samples). The Schmid factor of the {10–12} tensile twin is quantitatively counted and shown in Fig. 8. Since high Schmid factor is beneficial for the activation of the tensile twin, we focus on the Schmid factor that is higher than 0.4.

For re-compression along the RD, the distribution of the Schmid factor of {10–12} twin in CN-5% and CN-10% is very similar with that in the as-received sample, as indicated in Fig. 8(a). However, Fig. 4 indicates that the twin number density in CN-5%-CR-10% sample (50.5%) and CN-10%-CR-10% sample (71.7%) are obviously higher than that in CR-10% (36.5%). This implies that the small pre-deformation (5% and 10%) induced enhancement effect on the twinning in re-compression along the RD is not mainly related with the crystallographic orientation change because no obvious crystallographic orientation change is observed in the CN-5% and CN-10% sample. Some other mechanisms need to be further explored. After large pre-compression (20%) along the ND, the Schmid factor of {10–12} twin if compressing along the RD gets increase compared with that in the as-received sample, thus being beneficial for the twinning in the RD re-compression. So, when the pre-strain is large (20%), the pre-deformation induced crystallographic orientation change may contribute to the enhancement effect on twin activation during re-compression along the RD.

For re-compression along the TD, the distribution of Schmid factor of tensile twin in CN-5% is almost same as that in the as-received sample, as indicated in Fig. 8(b). However, when the applied strain is small (5%), Fig. 4 indicates that pre-compression (5%) along the ND will hinder the activation of tensile twin during re-compression along the TD. Fig. 8(b) implies this hindered effect is not mainly caused by the pre-deformation induced crystallographic orientation change. Some other mechanisms need to be further explored. With the increase of the pre-deformation (10% and 20%), the Schmid factor becomes higher than that in the as-received sample. And, the tensile twin activation during re-compression along the TD is also enhanced. In these cases, the pre-deformation induced orientation change may contribute to the enhancement effect on the twin activation during re-compression along the TD.

4.2. Effect of grain boundary misorientation on the twinning during re-compression

The effect of the pre-deformation along the ND on the subsequent twinning can not be fully explained by the crystallographic orientation change. L. Capolungo et al. [5] reported that the twins in Zr alloy nucleated preferentially at grain boundary with relative low misorientation angle. The underlying mechanism may be that the strain produced by the twin can be more easily accommodated in the neighbouring grain if the misorientation angle is relative small [34,35]. In this work, the grain boundary misorientation may be changed by the pre-deformation, which then affects the nucleation of twins during re-compression.

Whether the {10–12} tensile twin in Zr702 alloy prefers to nucleate at grain boundary with low misorientation angle is firstly checked. The distributions of misorientation angle of grain boundaries and the twin boundary in CR-10% and CT-10% samples are shown in Fig. 9. It can be observed from Fig. 9 that majority twin boundaries are intersected with grain boundaries. The intersection point between the twin boundary and the grain boundary can be roughly recognized as the nucleation location for the twin [36–38]. The misorientation angle of grain boundary, at which {10–12} twins have nucleated, are counted and presented Fig. 10.

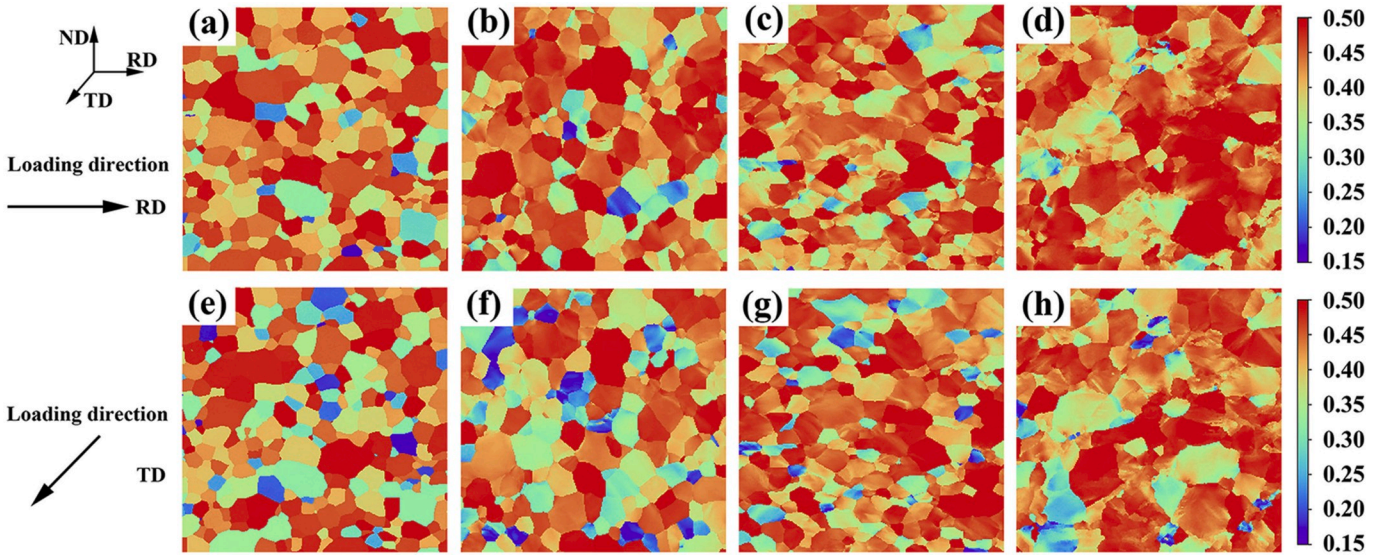

Fig. 7. Schmid factor distribution map of {10–12} twin in (a) as-received, (b) CN-5%, (c) CN-10% and (d) CN-20% if compressing along the RD, Schmid factor distribution map of {10–12} twin in (e) as-received, (f) CN-5% and (g) CN-10% and (h) CN-20% if compressing along the TD. Schmid factors are computed based on the orientation maps shown in Fig. 1(a) (as-received sample) and Fig. 2(a)–(c) (pre-compressed samples).

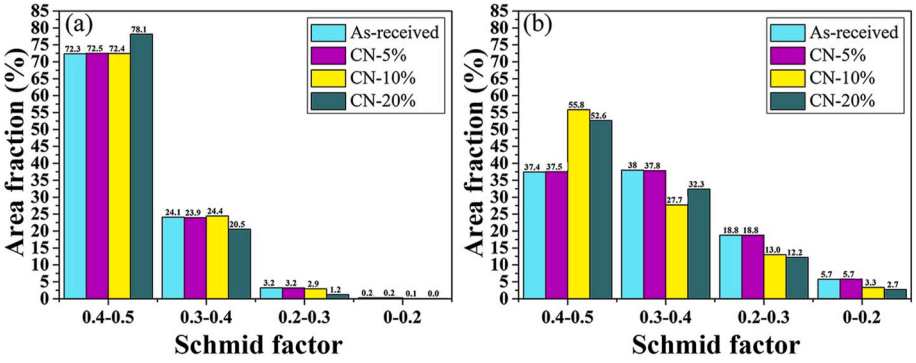

Fig. 8. Schmid factor distribution map of {10–12} twin in the as-received and pre-compressed samples if compressing along the (a) RD and (b) TD.

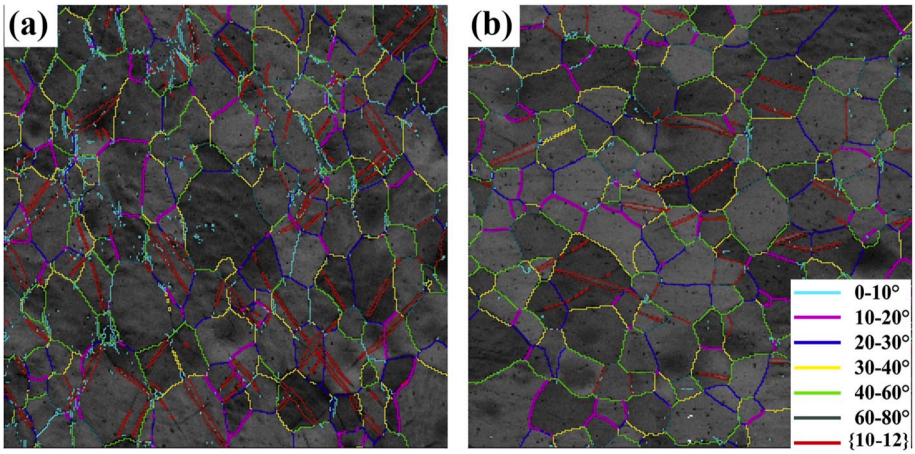

Fig. 9. Band contrast maps superimposed with twin boundary and misorientation angle of grain boundary in (a) CR-10% and (b) CT-10% sample.

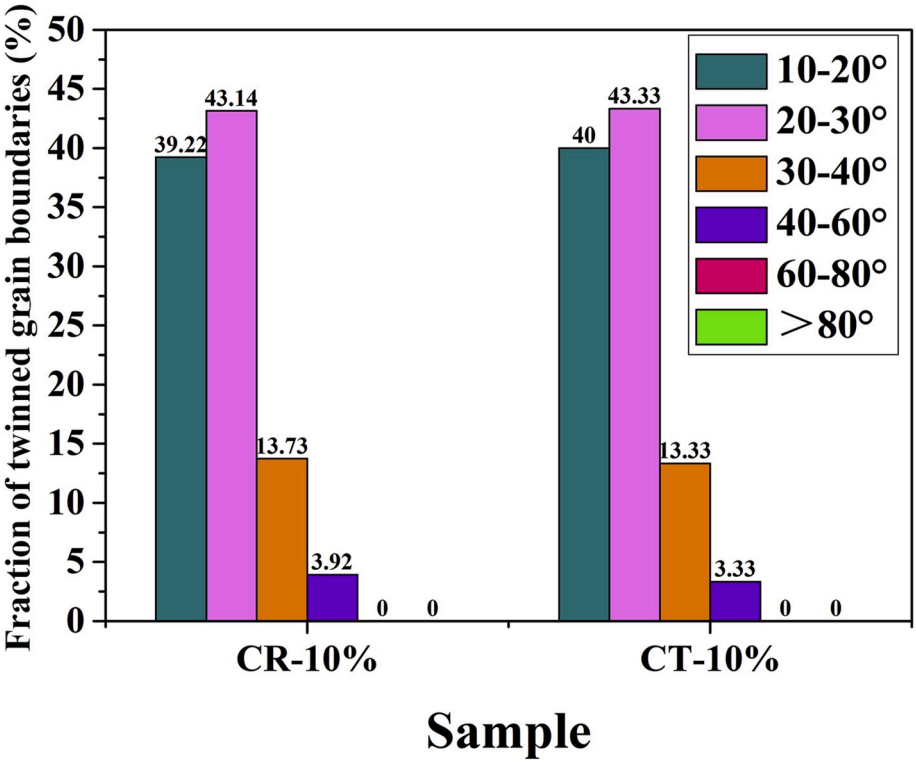

Fig. 10. The fraction of misorientation angles of grain boundary, where having twin nucleation.

It indicates that the fraction for twins nucleated at grain boundary with misorientation angle between 10-20° and 20-30° are significantly higher than other misorientation angles. This validates that the {10–12} twins in Zr702 alloy indeed tend to preferentially nucleate at grain boundary with low misorientation angle.

Then, the effect of the pre-deformation along the ND on the misorientation angles of grain boundaries are checked. The misorientation angles of grain boundaries in the as-received and the pre-compressed samples are shown in Fig. 11. The fractions of grain boundary with different misorientation angles (>10°) are counted and presented in Fig. 12. Compared with the as-received sample, the fraction of the grain boundary with low misorientation angle (10^{o}-20°) increases (from~10% to ~25%) with the increase of the pre-deformation along the ND, especially when the pre-deformation is higher than 10%. Therefore, the pre-deformation along the ND has increased the length fraction of the grain boundary with relative low misorientation angle (10^{o}-20°), which may provide more nucleation locations for the {10–12}, thus enhancing the twinning in subsequent re-compression along the RD or TD.

However, the increase of the grain boundary with low misorientation angle (>10°) is not obvious when the pre-deformation is small (5%). It may be not the main reason that causing the enhanced twin activation in CN-5%-CR-10% sample. In addition, the twinning in the re-compression along the TD is actually hindered by the small pre-deformation (5%). Therefore, some other mechanisms need to be further explored. Moreover, high density of low angle sub-boundary (with misorientation angle <10°) can be noted in ND pre-compressed samples, especially at large pre-deformation (20%). It is assumed that the low angle sub-boundary affects the subsequent twinning by local stress accumulation, which is discussed in next section.

4.3. Effect of local stress concentration on the twinning

The effect of the ND pre-deformation on the subsequent twinning can not be fully explained by the change in orientation and the change in misorientation angle of grain boundary. Yang et al. [30] reported that some of the observed twins in uniaxial tension were not activated in accordance with the Schmid law. Complex local stress was assumed to be the main mechanism to activate these non-schmid-twins [30]. The local stress is closely related with inhomogeneous deformation between grains due to different initial grain orientation.

In the current study, intra and inter granular residual local stress

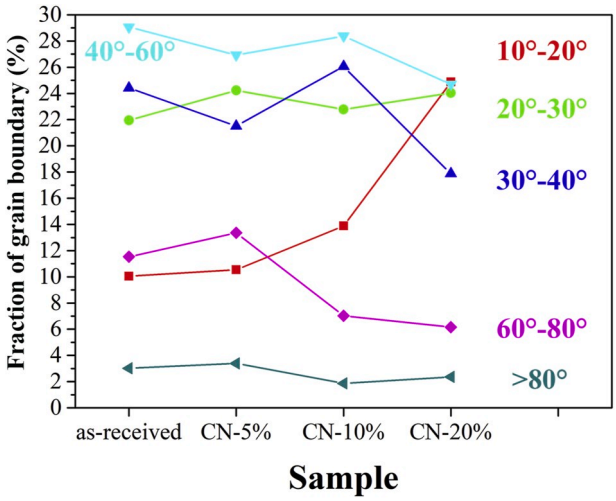

Fig. 12. Distribution of misorientation angle (>10°) of grain boundary in the as-received sample and the pre-compressed samples.

must be formed during the pre-compression along the ND, which may affect the subsequent twinning in re-compression along the RD or TD. Non-uniformly distributed low angle (<10°) grain boundaries, as shown in Fig. 11(b)–(d), reflect the non-uniform deformation (thus complex local stress). To check the effect of local stress concentration induced by the pre-deformation on the subsequent twinning, non-schmid-twin is analyzed. It is worth to note that the non-schmid-twin is defined as that the activated twin variants do not have the maximum schimid factor with respect to the macroscopic loading stress. As shown in Fig. 13, the activated typical twin variants are marked near the twin lamella. The schmid factor values of all variants are calculated and listed in Fig. 13. The Schmid factor values for the activated twin variants are emphasized by red color. It indicates that many twins belong to non-schmid-twins.

The ratio of non-schmid-twins with respect to all twins in the single-step compressed and two-step compressed samples are counted and presented in Fig. 14. It indicates that the pre-compression along the ND indeed increases the fraction of non-schmid-twin when re-compression along the RD despite the applied strain level. When the pre-strain is higher than 10%, the fraction of the non-schmid-twin gets also increased when re-compression along the TD. That means the local stress

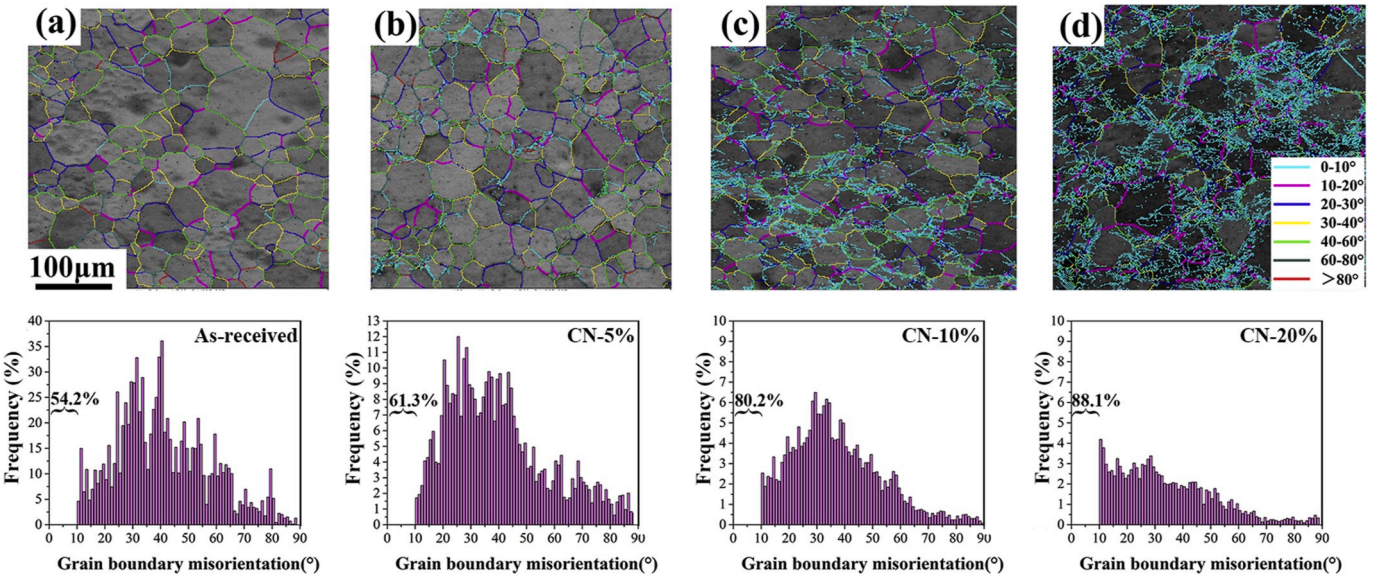

Fig. 11. Band contrast maps superimposed with misorientation angle of grain boundary in the (a) as-received, (b) CN-5%, (c) CN-10% and (d) CN-20%.

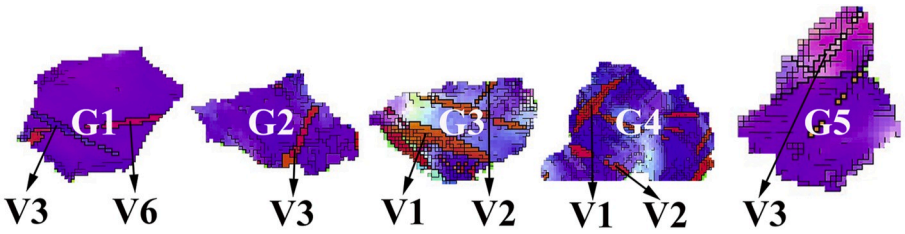

Variants	Schmid factor				
	G1	G2	G3	G4	G5
V1	-0.022	-0.021	0.128	0.183	-0.068
V2	-0.062	0.263	0.176	0.191	-0.033
V3	-0.072	0.215	0.286	0.213	0.195
V4	-0.036	0.333	0.291	0.245	0.269
V5	0.185	-0.016	-0.012	0.012	-0.052
V6	0.162	0.218	-0.029	0.036	-0.013

Fig. 13. Activated twin variants and Schimd factor values of all possible twin variants.

concentration contributes to the pre-deformation enhancement for subsequent twinning in re-compression. However, it is still unclear why the small pre-deformation (5%) hinders the subsequent twinning when re-compression along the TD.

4.4. Hindering effect of the small pre-deformation on the twinning in re-compression along the TD

When the pre-compression is small (5%), Fig. 4 indicates that the twinning in re-compression along the TD is hindered, which can not be reasonably explained by the mentioned texture change, local stress concentration and misorientation. It may be related with the anisotropy as results of the initial split basal texture. It is accepted that the main deformation modes of Zr alloy at room temperature are prismatic <a> slipping, pyramidal <c+a> slipping and {10–12} tensile twinning [7, 10,32]. In addition, the critical resolved shear stress (CRSS) are ordered like: prismatic <a> < {10–12} tensile twin < pyramidal <c+a> [39].

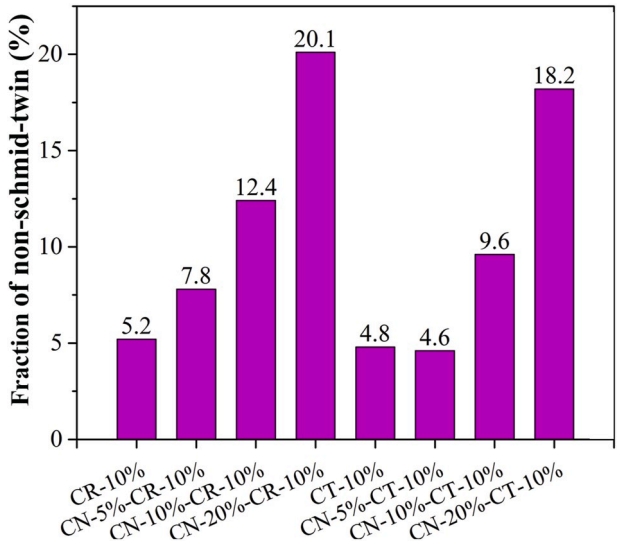

Fig. 14. The fraction of non-schmid-twin with respect to all twins in single-step compressed and two-step compressed samples.

For single-step compression tests, the Schmid factor of {10–12} twin is relatively higher for compression along the RD than that along the TD as results of the tilted basal pole to the TD, as shown in Fig. 8. While, the Schmid factor of pyramidal <c+a> for compression along the RD is smaller than that along the TD. During single-step compression along the RD, the main deformation modes are prismatic <a> slipping and tensile twinning. While, compared with the compression along the RD, much more pyramidal <c+a> slipping must be activated during compression along the TD, which causes the higher initial yield strength, as indicated in Fig. 15 ($\sigma_{yield\text{-}CT}$ = 429 MPa > $\sigma_{yield\text{-}CR}$ = 366 MPa). It is worthy to note that the initial yield strength in the current work is defined as the 0.6% offset flow strength on the engineering stress-strain curve considering that the elastic deformation of the testing machine being involved in the stress-strain curve without using extensometer. And, the selection of offset strain (0.2%, 0.6% or 0.8% for instance) to determine the initial yield strength will not affect subsequent discussions and the main conclusion.

In the pre-compression along the ND, as mentioned before, the main deformation modes are prismatic <a> and pyramidal <c+a> slipping [32,33] The pre-deformation induced dislocations lead to the work hardening phenomenon when re-compression along the RD or TD compared with the single-step compression, as indicated in Fig. 15. However, the amounts of work hardening are different when re-compression along different directions. As indicated in Fig. 15, when re-loading along the RD, the amount of work hardening is ~109 MPa. While, it is ~50 MPa for re-compression along the TD. It implies that the work hardening mechanisms are different for re-compression along the RD and the TD. It is worth to note that the main deformation modes (prismatic <a> and pyramidal <c+a> slipping) in the re-compression along the TD are similar with that in the pre-compression along the ND. So, it is speculated that many of prismatic<a> and pyramidal <c+a> dislocations induced by the small pre-deformation (5%) are still moveable in re-compression along the TD, which may help to partially cancel out the work hardening because less new dislocation sources need to be activated compared with that in single-step compression for a given accumulated strain. In contrast, new deformation mode (tensile twinning) is activated to accommodate the applied RD re-compression, thus leading to a higher amount of work hardening.

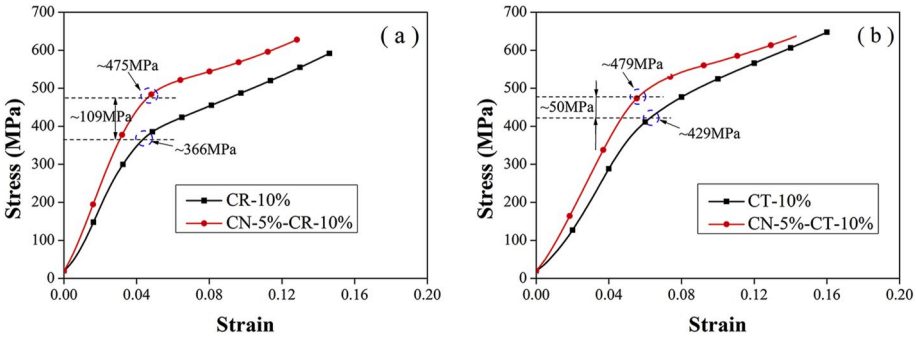

Fig. 15. Typical engineering stress-strain curves of single-step compressed samples and two-step compressed samples.

In summary, during the pre-deformation along the ND, pyramidal <c+a> slipping is activated and partially kept as movable in the re-compression along the TD. So, compared with the single-step compression at same accumulated strain, the contribution of pyramidal <c+a> slipping to the deformation may be relative higher in the re-compression along the TD, thus leading to fewer twin activation. With the further increase of the pre-deformation, the density of the dislocation is very high, which makes it hard to keep movable for the pre-induced dislocation in re-compression. However, the speculation that the pre-induced dislocations keep still movable in the subsequent re-compression needs further evaluation in future work.

Above all, grain orientation, misorientation angle of grain boundary and local stress may be changed by the ND pre-deformation, thus affecting the twinning in subsequent re-compression. However, the quantitative contribution of each factor is not discussed in this study because these factors are tightly coupled together. The initial crystallographic orientation of Zr702 plate varies among grains. Under pre-deformation, the plastic deformation varies from grain to grain, which causes the rotation of crystallographic orientation and complex local stress. At the same time, the non-uniform rotation of grain orientation may be accompanied by misorientation change. Quantitative contribution of different factors to the subsequent twinning needs to be further explored in future work based on more ex- or in-situ experimental data.

5. Conclusions

In this work,two steps of compressions are performed on a Zr702 alloy to reveal the effect of pre-deformation on twinning in subsequent compression. Microstructures and texture after compression are observed by EBSD. The primary conclusions obtained are as follows:

(1) Pre-compression along the ND will enhance the activation of {10–12} twin in re-compression along the RD despite the applied pre-strain level. The larger the pre-compression, the more significant the enhancement effect is. This enhancement effect may be attributed to the crystallographic orientation change, the increase of grain boundary with low misorientation angle and the local stress concentration caused by the pre-deformation in the ND.

(2) Small pre-deformation along the ND will hinder the twinning in re-compression along the TD, while large pre-deformation will enhance the twinning in re-compression along the TD. The large pre-deformation enhanced twinning in re-compression along the TD may also relate with the crystallographic orientation change, the increase of grain boundary with low misorientation angle and the local stress concentration. The hindering effect of the small pre-deformation may be attributed to the anisotropy of the textured Zr702 sheet and the strain path change effect.

Declaration of competing interest

The authors declare that they have no known competing financial interests or personal relationships that could have appeared to influence the work reported in this paper.

CRediT authorship contribution statement

Xin Chen: Data curation, Investigation, Validation, Writing - original draft, Writing - review & editing. **Qinghui Zeng:** Investigation, Formal analysis, Writing - review & editing. **Weijun He:** Conceptualization, Formal analysis, Investigation, Writing - review & editing, Funding acquisition, Supervision. **Qing Liu:** Funding acquisition, Supervision, Writing - review & editing.

Acknowledgements

The authors express their sincere thanks for the financial support from the National Natural Science Foundation of China (Projects 51971041, 51601023 and 51421001 and Natural Science Foundation of Chongqing (Projects No. cstc2019jcyj-msxmX0234).

References

[1] J.A.L. Robertson, Zirconium-an international nuclear material, J. Nucl. Mater. 100 (1981) 108–118.
[2] S. Banerjee, M.K. Banerjee, Nuclear applications: zirconium alloy, Mater. Sci. Mater. Eng. (2016) 6287–6299.
[3] L. Chai, B. Luan, K.L. Murty, Effect of predeformation on microstructural evolution of a Zr alloy during 550–700°C aging after β quenching, Acta Mater. 61 (2013) 3099–3109.
[4] L. Capolungo, I.J. Beyerlein, C.N. Tomé, On the interaction between slip dislocations and twins in HCP Zr, Mater. Sci. Eng. 513–514 (2009) 42–51.
[5] L. Capolungo, P.E. Marshall, C.N. Tomé, Nucleation and growth of twins in Zr: a statistical study, Acta Mater. 57 (2009) 6047–6056.
[6] L. Chai, B. Chen, Z. Zhou, W. Huang, A special twin relationship or a common Burgers misorientation between α plates after β quenching in Zr alloy? Mater. Char. 104 (2015) 61–65.
[7] M. Zhang, B.F. Luan, Q. Liu. {11-21}-{10-12}double twinning in a Zircaloy-4 alloy during rolling at ambient temperature, Scripta Mater. 122 (2016) 77–81.
[8] B.F. Luan, L.J. Chai, G.L. Wu, H.B. Yu, J.W. Chen, Q. Liu, Twinning during β→α slow cooling in a zirconium alloy, Scripta Mater. 67 (2012) 716–719.
[9] R.A.L.C.N. Tome, A model for texture development dominated by deformation twinning application to zirconium alloys, Acta Metall. Mater. 39 (1991) 2667–2680.
[10] W.J. He, X. Chen, H. Chen, Q. Liu, Grain size effect on the thermally activated twin boundary migration in a zirconium alloy, Materials Science and Engineering: A 724 (2018) 576–585.
[11] Q. Wang, C. Cochrane, T. Skippon, Z. Wang, H. Abdolvand, M.R. Daymond, Orientation-dependent irradiation hardening in pure Zr studied by nanoindentation, electron microscopies, and crystal plasticity finite element modeling, Int. J. Plast. 124 (2020) 133–154.
[12] A. Harooni, M. Iravani, A. Khajepour, J.M. King, A. Khalifa, A.P. Gerlich, Mechanical properties and microstructures in zirconium deposited by injected powder laser additive manufacturing, Additive Manufacturing 22 (2018) 537–547.
[13] Z.N. Yang, Y.Y. Xiao, F.C. Zhang, Z.G. Yan, Effect of cold rolling on microstructure and mechanical properties of pure Zr, Materials Science and Engineering: A 556 (2012) 728–733.

[14] J. Hu, L. Yang, G. Cao, Y. Yun, G. Yuan, Q. Yue, G. Shao, On the oxidation behavior of (Zr,Nb)2Fe under simulated nuclear reactor conditions, Corros. Sci. 112 (2016) 718–723.
[15] S. Banerjee, M.K. Banerjee, Corrosion of zirconium and its alloys, Material Science and Material Engineering (2016) 6287–6299.
[16] O.T. Woo, D. Tseng, K. Tangri, S.R. MacEwen, Flow stress and dynamic strain-ageing of β-transformed Zircaloy-4, J. Nucl. Mater. 87 (1979) 135–143.
[17] G.G. Yapici, C.N. Tomé, I.J. Beyerlein, I. Karaman, S.C. Vogel, C. Liu, Plastic flow anisotropy of pure zirconium after severe plastic deformation at room temperature, Acta Mater. 57 (2009) 4855–4865.
[18] G.B. Reddy, R. Kapoor, A. Sarkar, Probability based ranking approach for twin variant selection in an α-Zr alloy, Int. J. Plast. 122 (2019) 164–187.
[19] J.H. Chung, Development of thermomechanical processing method to enhance twinning in commercially pure Zr, Scripta Mater. 61 (2009) 161–164.
[20] O. Muránsky, M.R. Daymond, D. Bhattacharyya, O. Zanellato, S.C. Vogel, L. Edwards, Load partitioning and evidence of deformation twinning in dual-phase fine-grained Zr–2.5%Nb alloy, Mater. Sci. Eng. 564 (2013) 548–558.
[21] M. Knezevic, M. Zecevic, I.J. Beyerlein, J.F. Bingert, R.J. McCabe, Strain rate and temperature effects on the selection of primary and secondary slip and twinning systems in HCP Zr, Acta Mater. 88 (2015) 55–73.
[22] W.J. He, X. Chen, Q. Liu, Effect of pre-annealing deformation on thermally activated twin boundary migration in a zirconium alloy, J. Alloys Compd. 742 (2018) 29–37.
[23] J. Wang, J.P. Hirth, C.N. Tomé, {10-12} Twinning nucleation mechanisms in hexagonal-close-packed crystals, Acta Mater. 57 (2009) 5521–5530.
[24] Jing Tang, Haidong Fan, Wei Dean, Wentao Jiang, Qingyuan Wang, Xiaobao Tian, Xu Zhang, Interaction between a {10-12} twin boundary and grain boundaries in magnesium, Internatinal Journal of Plasticity 126 (2020) 102613.
[25] H. Somekawa, Hall–Petch relation for deformation twinning in solid solution magnesium alloys, Materials Science and Engineering: A (Structural Materials: Properties, Microstructure and Processing) 561 (2013) 378–385.
[26] Seong-Woo Choia, Jong Woo Wonl, Deformation twinning activity and twin structure development of pure titanium at cryogenic temperature, Mater. Sci. Eng. 738 (2018) 75–80.
[27] Xinglong An, Hao Zhang, Song Ni, Xiaoqin Ou, Xiaozhou Liao, Min Song, Effects of temperature and alloying content on the phase transformation and {10-11} twinning in Zr during rolling, J. Mater. Sci. Technol. 4115 (2020) 76–80.
[28] S.G. Hong, S.H. Park, C.S. Lee, Strain path dependence of {10-12} twinning activity in a polycrystalline magnesium alloy, Scripta Mater. 64 (2011) 145–148.
[29] Hong Qin, John J. Jonas, Hongbing Yu, Nicolas Brodusch, Raynald Gauvin, Xiyan Zhang, Initiation and accommodation of primary twins in high-purity titanium, Acta Mater. 71 (2014) 293–305.
[30] H.L. Yang, S. Kano, L.J. Chai, J.J. Shen, Z.S. Zhao, J. McGrady, Z.G. Duan, H. Abe, Interaction between slip and {10-12} tensile twinning in Zr alloy: quasi in situ electron backscatter diffraction study under uniaxial tensile test, J. Alloys Compd. 782 (2019) 659–666.
[31] Jing Chen, Yilan Jiang, Huiqun Liu, Danqing Yi, Ruiqian Zhang, Texture evolution of cold-rolled Zr-1Sn-0.3Nb-0.3Fe-0.1Cr alloy during annealing, J. Nucl. Mater. 524 (2019) 226–238.
[32] W.J. He, Adrien Chapuis, Xin Chen, Qing Liu, Effect of loading direction on the deformation and annealing behavior of a zirconium alloy, Mater. Sci. Eng. 734 (2018) 364–373.
[33] O. Castelnaua, H. Francilletteb, B. Bacroixa, R.A. Lebensohn, Texture dependent plastic behavior of Zr 702 at large strain, J. Nucl. Mater. 297 (2001) 14–26.
[34] J.J. Jonas, Mu Sijia, Talal Al-Samman, et al., The role of strain accommodation during the variant selection of primary twins in magnesium, Acta Mater. 59 (2011) 2046–2056.
[35] H. Qin, J. J, Jonas, H. Yu, N. Brodusch, R. Gauvin, X. Zhang, Initiation and accommodation of primary twins in high-purity titanium, Acta Mater. 71 (2014) 293–305.
[36] Bingshu wang, Jingjing Shi, Qiang Liu, In-situ investigation on nucleation and propagation of {10-12} twins during uniaxial multi-pass compression in an extruded AZ31 Mg alloy, Mater. Sci. Eng. 731 (2018) 71–79.
[37] Xin Wan, Jing Zhang, Xueyan Mo, Yu Luo, Effects of pre-strain on twinning behaviors in an extruded Mg-Zr alloy, Mater. Sci. Eng. 766 (2019) 138335.
[38] Y. Xin, L. Lv, H. Chen, C. He, H. Yu, Q. Liu, Effect of dislocation-twin boundary interaction on deformation by twin boundary migration, Materials Science and Engineering: A 662 (2016) 95–99.
[39] J.W. Christian, S. Mahajan, Deformation twinning, Prog. Mater. Sci. 39 (1) (1995) 1–157.